

## Electronic supplementary information

for

### In situ formation of surface and bulk oxides in small palladium nanoparticles

Aram L. Bugaev,<sup>\*a,b</sup> Maxim Zabilskiy,<sup>c</sup> Alina A. Skorynina,<sup>a</sup> Oleg A. Usoltsev,<sup>a</sup>  
Alexander V. Soldatov,<sup>a</sup> Jeroen A. van Bokhoven<sup>c,d</sup>

<sup>a</sup>The Smart Materials Research Institute, Southern Federal University, Sladkova 178/24, 344090, Rostov-on-Don, Russia

<sup>b</sup>Southern Scientific Centre, Russian Academy of Sciences, Chekhova 41, 344006 Rostov-on-Don, Russia

<sup>c</sup>Laboratory for Catalysis and Sustainable Chemistry, Paul Scherrer Institute, 5232 Villigen, Switzerland

<sup>d</sup>Institute for Chemical and Bioengineering, ETH Zurich, Vladimir-Prelog-Weg 1, 8093 Zurich, Switzerland

\*Email: abugaev@sfedu.ru

#### Table of contents

Catalyst synthesis.....	2
Scanning transmission electron microscopy (STEM).....	2
X-ray diffraction (XRD) .....	3
Volumetric measurements .....	3
Chemisorption measurements.....	4
In situ synchrotron studies .....	5
Temperature increase during H <sub>2</sub> oxidation .....	9
References.....	9

## Catalyst synthesis

To prepare  $\gamma$ -alumina, 10 g of commercially available Boehmite (Capatal® B Alumina, Sasol) was calcined in air at 600 °C for 8 h (heating ramp 10 °C/min). The following method was applied to deposit 1 wt. % of palladium over  $\gamma$ -alumina support. 6 g of  $\gamma$ -alumina was impregnated with solution of Pd<sup>2+</sup> prepared by dissolution of 253 mg of Pd(NO<sub>3</sub>)<sub>2</sub>·2H<sub>2</sub>O (99% purity, SigmaAldrich) in 8 ml of deionized water, followed by addition of 0.88 g of 28 wt. % ammonia solution (Aldrich). Sample was dried overnight at 110 °C and then calcined in air at 350 °C for 5 hours (heating ramp 2 °C/min). After that, material was reduced for 2 hours in a flow of gas mixture containing 5 vol. % of H<sub>2</sub> in Argon (flowrate: 50 mL/min) at 260 °C (heating ramp 2 °C/min).

## Scanning transmission electron microscopy (STEM)

STEM images were obtained on a probe-corrected Hitachi HD2700CS microscope equipped with a high-angle annular dark field (HAADF) detector and an energy-dispersive detector (EDX).

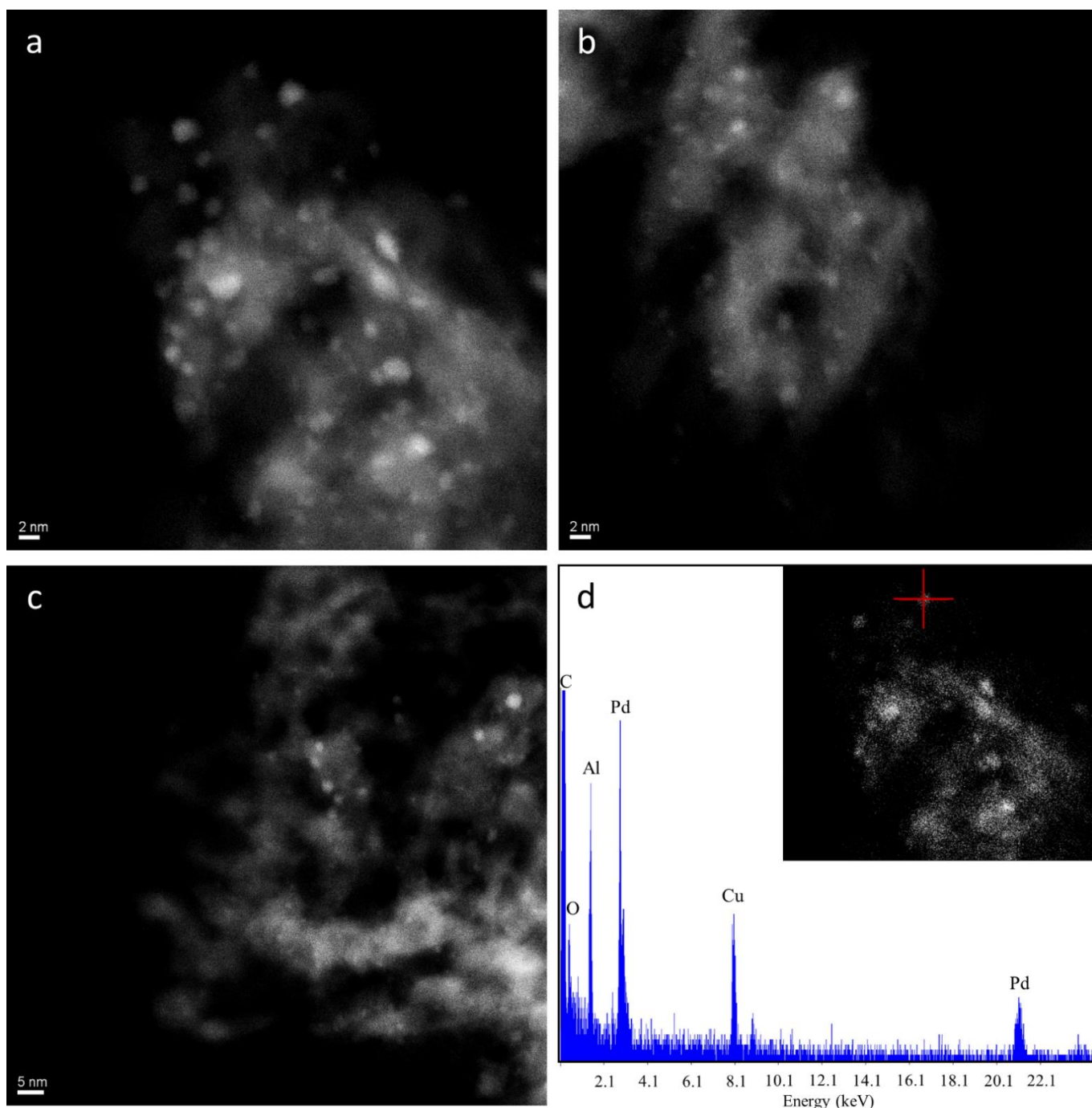


**Figure S1.** (a-c) Series of HAADF-STEM micrographs of Pd/Al<sub>2</sub>O<sub>3</sub> sample. (d) EDX analysis.

## X-ray diffraction (XRD)

XRD measurements were performed at room temperature on a Bruker D8 Advance AXS diffractometer using Cu  $K_{\alpha 1}$  radiation with  $\lambda = 0.15406$  nm. Materials were scanned in the  $2\theta$  range between 20 to 80° with 0.021° increment and 1 s acquisition time at each point.

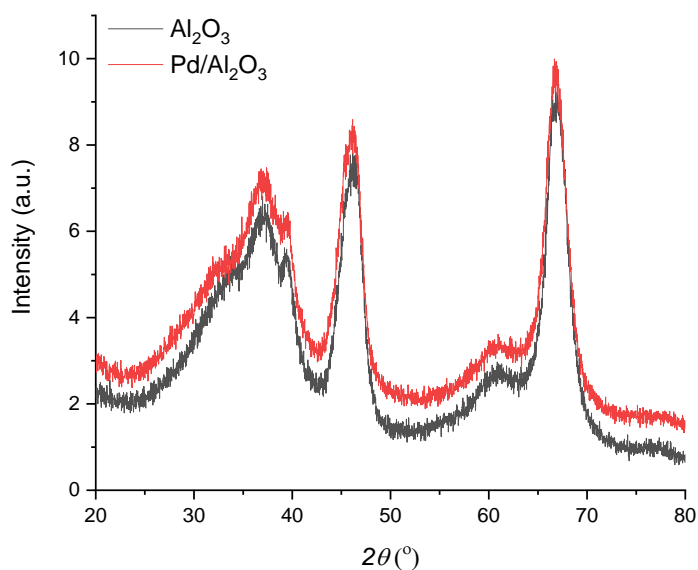


**Figure S2.** XRD patterns of  $\gamma$ -alumina support and synthesized Pd/ $\text{Al}_2\text{O}_3$  catalyst.

## Volumetric measurements

BET specific surface area, total pore volume and pore size distribution were determined at  $-196$  °C using 3Flex Surface Characterization Analyzer manufactured by Micromeritics. Prior to measurement, Pd/ $\text{Al}_2\text{O}_3$  sample was evacuated at 110 °C for 1 h, followed by 3 h soaking under vacuum at 300 °C (heating ramp 2 °C/min) using the Micromeritics SmartPrep degasser. The Brunauer-Emmett-Teller (BET) method was applied to calculate specific surface area. The pore size distribution was derived from the desorption branch of the isotherms employing the Barrett-Joyner-Halenda (BJH) method. The total pore volume was estimated at a relative pressure of 0.99.

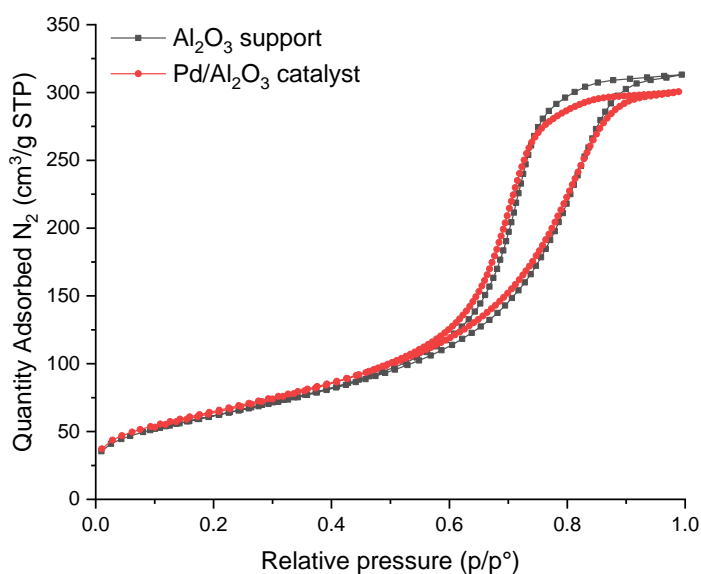


**Figure S3.** Nitrogen adsorption–desorption isotherms of  $\gamma$ -alumina support (black squares) and synthesized Pd/ $\text{Al}_2\text{O}_3$  catalyst (red circles).

## Chemisorption measurements

H<sub>2</sub> chemisorption was performed by using Micromeritics 3Flex Surface Characterization Analyzer. Synthesized Pd/Al<sub>2</sub>O<sub>3</sub> material was firstly degassed at 100 °C in vacuum for 1 h. After that, the sample was reduced in a flow of hydrogen at 250 °C for 1 h, followed by evacuation at 250 °C for 3 h. H<sub>2</sub> adsorption isotherms were measured at 35 °C. During the measurements, small doses of hydrogen (0.1 cm<sup>3</sup>·g<sup>-1</sup>) were equilibrated to acquire high-resolution adsorption isotherm. After finishing the first adsorption isotherm, the sample was evacuated at 35 °C for 1 h (to remove weakly adsorbed hydrogen), and the measurement of H<sub>2</sub> isotherm was repeated in order to estimate the amount of physically adsorbed hydrogen. Dispersion of palladium and average nanoparticle size were calculated by i) extrapolating both adsorption isotherms to zero pressure and ii) applying difference method to calculate the amount of irreversibly chemisorbed hydrogen. For particle size calculation, it was assumed that palladium nanoparticles possess semispherical geometry and adsorption stoichiometry of H<sub>2</sub>/Pd = 2.

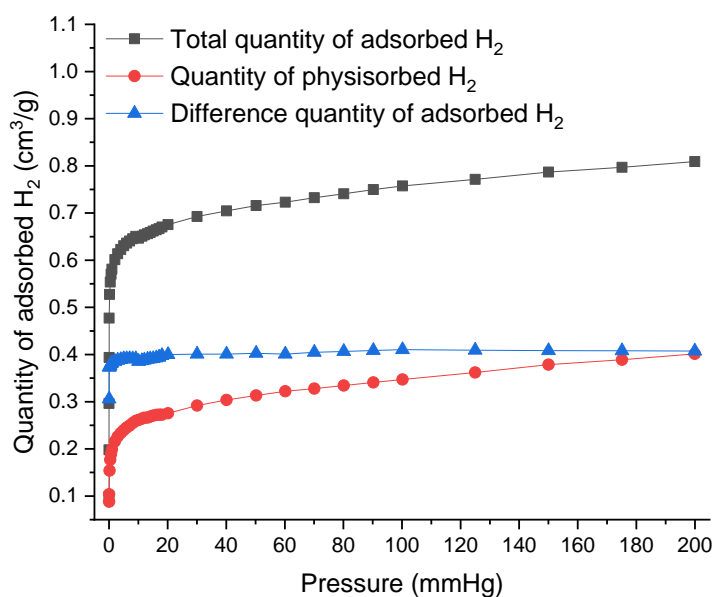


**Figure S4.** Hydrogen adsorption isotherms of Pd/Al<sub>2</sub>O<sub>3</sub> catalyst measured at 35 °C.

**Table S1.** Physico-chemical characterization of prepared Pd/Al<sub>2</sub>O<sub>3</sub> catalyst and  $\gamma$ -alumina support.

Sample	BET (m <sup>2</sup> /g)	Pore volume (cm <sup>3</sup> /g)	Pd loading, (wt. %)	Pd dispersion (%)	Average particle size (nm)	
					TEM	H <sub>2</sub> chemisorption
$\gamma$ -alumina	224	0.48	-	-	-	-
Pd/Al <sub>2</sub> O <sub>3</sub>	236	0.46	0.8	48	1.9	2.3

## In situ synchrotron studies

*In situ* X-ray absorption spectroscopy (XAS) measurements were performed at BM31 beamline<sup>1</sup> of ESRF (Grenoble, France). The sample was sieved to the grain size of 100 – 160  $\mu\text{m}$  and loaded into a 2 mm quartz glass capillary (ca. 14 mg of sample) fixed with a quartz wool from both sides. The capillary was glued into a metal sample-holder connected to a remotely controlled gas panel permanently installed at BM31. The gas feeds of  $\text{H}_2$ ,  $\text{O}_2$  and buffer He through the sample were set using mass flow controllers (Bronkhorst). The heat gun was located below the sample to control the temperature that was initially calibrated by a thermocouple inserted inside the capillary with the sample (without XAS measurements). The outgoing gas mixture after the sample was monitored by Pfeiffer OmniStar GSD 320 mass spectrometer. XAS measurements were performed in the transmission mode using Si (111) double crystal monochromator detuned to 70% to reduce the contribution of the 3<sup>rd</sup> harmonic. The spectra were processed in Demeter code in a standard way.<sup>2</sup> One Pd–O and two Pd–Pd paths (see Table S2) were included in the fitting model with independent interatomic distances  $R$ , but with coordination numbers  $N$  derived from the size equation<sup>3</sup> with only one variable (particle size) for all three paths.

**Table S2.** Structural parameters of the initial palladium oxide phase determined by EXAFS analysis.

Path	$R, \text{\AA}$	$N$	$\sigma^2, \text{\AA}^2$
Pd–O	$2.01 \pm 0.01$	$3.1 \pm 0.2$	$0.002+0.001$
Pd–Pd (1)	$2.67 \pm 0.01$	$0.5 \pm 0.1$	$0.004+0.003$
Pd–Pd (2)	$3.22 \pm 0.02$	$0.6 \pm 0.1$	$0.004+0.003$

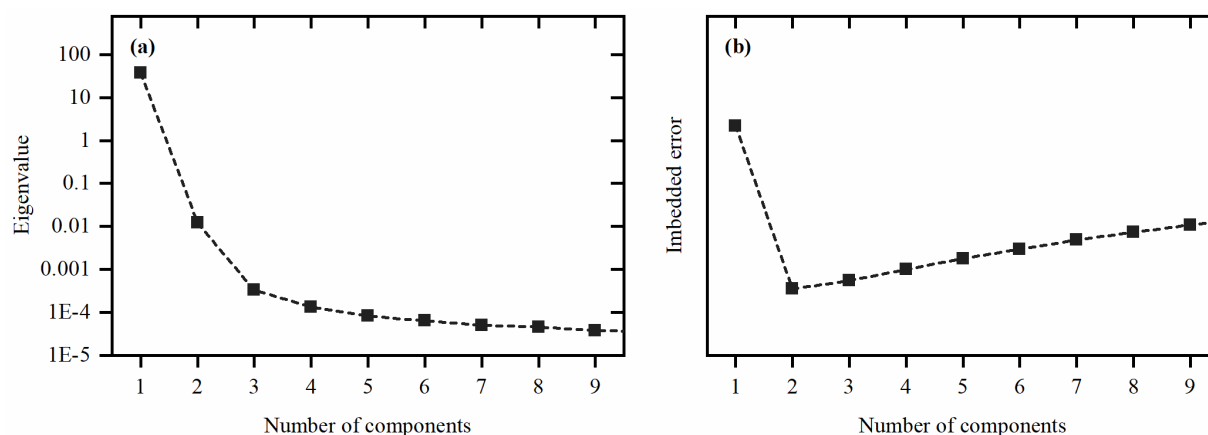


**Figure S5.** Scree plot (a) and imbedded error (IE) function (b) determined by PCA analysis of the whole dataset of XANES spectra.

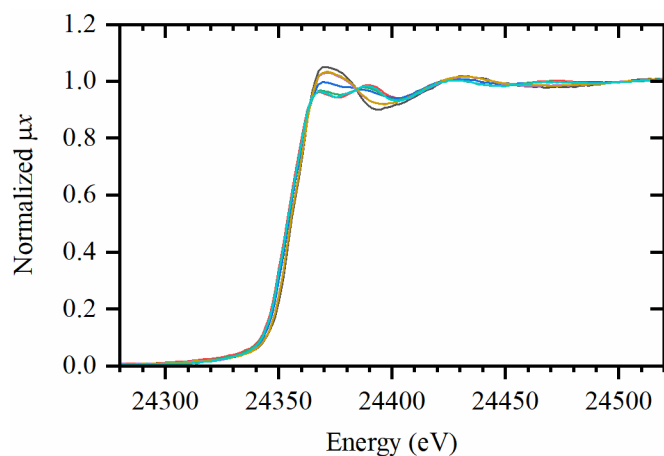


**Figure S6.** The same spectra shown in Figure 3c of the main text but plotted without vertical shift.

Bulk palladium oxide and oxidized carbon-supported palladium nanoparticles with average size of ca. 3 nm (provided by Chimet S.p.A.) were used as reference oxide samples. FT-EXAFS data shown in Figure S7 proves the nanometric dimensions of the studied Pd/Al<sub>2</sub>O<sub>3</sub> sample due to the absence of the signal above 2 Å, which is present for both bulk and 3 nm particles. In addition, the first-shell Pd-O signal in 1-2 Å region is also reduced in the studied Pd/Al<sub>2</sub>O<sub>3</sub> sample.

Carbon supported 3 nm nanoparticles were also successfully reduced by flowing 20% H<sub>2</sub>/He already at room temperature. XANES spectra shown in Figure S8 demonstrate that the reduction was complete, and no further reduction was observed after heating in hydrogen to 120 °C. The peaks shift between the red and blue curves in Figure S8 is due to the fact that at room temperature the hydride phase with increased cell parameter is formed, which is decomposed at 120 °C.

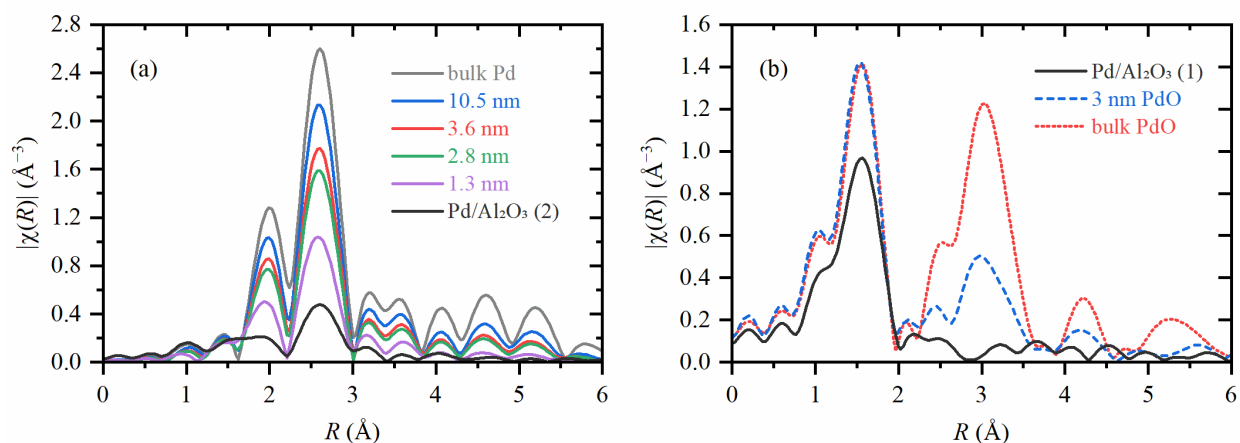


**Figure S7.** Experimental FT-EXAFS data. (a) The reduced state of Pd/Al<sub>2</sub>O<sub>3</sub> sample (solid black) compared to Pd foil (grey) and supported Pd nanoparticles with average sizes of 10.5 (blue), 3.6 (red), 2.8 (green) and 1.3 nm (purple), previously reported and analyzed in refs. 4, 5. (b) The initial (oxidized) state of Pd/Al<sub>2</sub>O<sub>3</sub> sample (solid black), 3 nm carbon-supported palladium nanoparticles after continuous exposure to air (dashed blue) and bulk palladium oxide (dotted red).

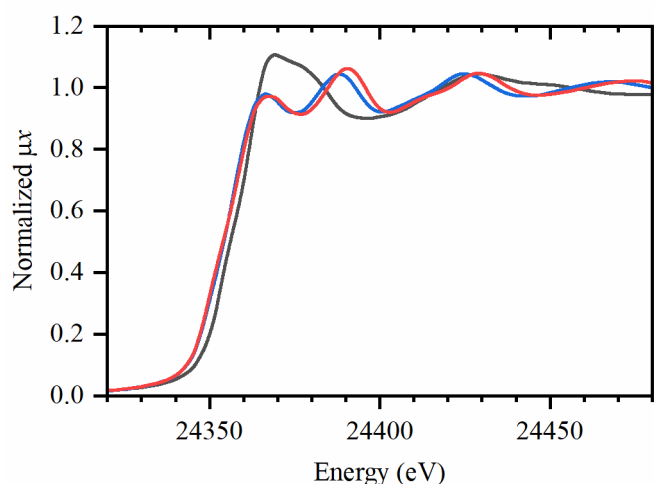


**Figure S8.** 3 nm carbon-supported palladium nanoparticles after continuous exposure to air (black), and in 20% H<sub>2</sub>/He at room temperature (blue) and at 120 °C (red).

To check the possibility of XANES for discrimination between Pd-O and Pd-OH species, theoretical XANES spectra were calculated in FDMNES code for Pd(111) surfaces and bulk structures (Figure S9). The optimal

geometry of surface adsorbed O and OH was obtained at DFT level of theory using VASP 5.3 code.<sup>6, 7</sup> The similarity of the PdO and Pd(OH)<sub>2</sub> species in XANES was also confirmed by experimental measurements on commercial reference samples (Figure S10).

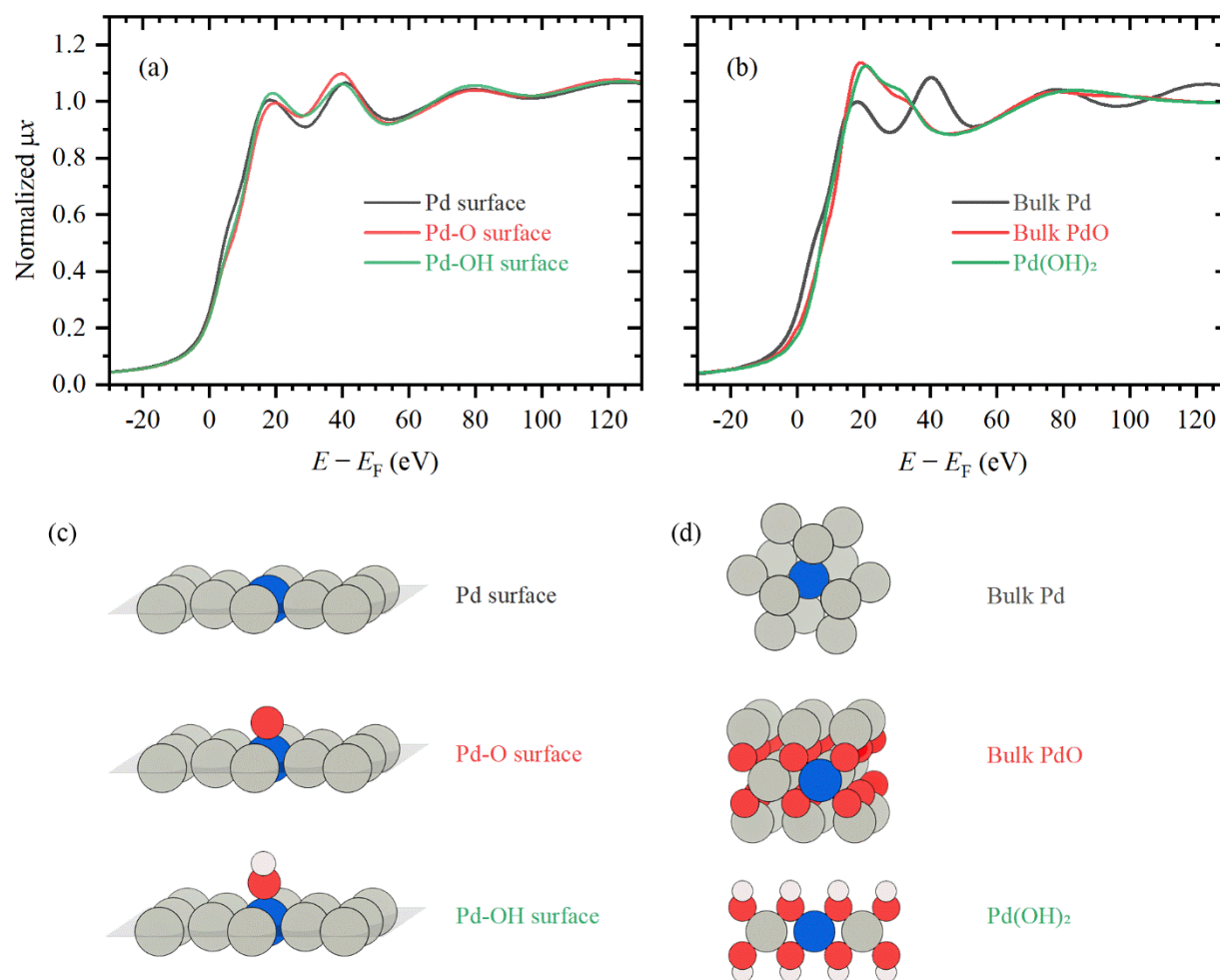


**Figure S9.** Theoretical XANES spectra for surface (a) and bulk (b) Pd-O (red) and Pd-OH (green) species. Parts (c) and (d) illustrate the atomic models (for visualization reason, only parts of the structures were made visible) used for XANES calculations with Pd, O, and H atoms colored in grey, red and white, respectively. The blue atoms correspond to palladium atoms for which XANES was calculated (absorbing atoms).

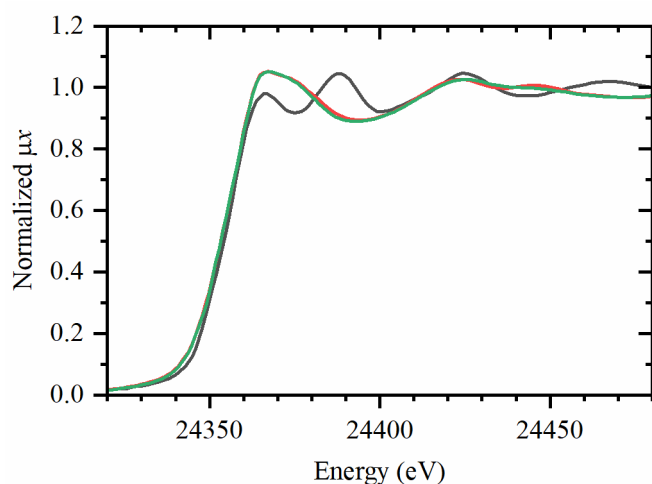


**Figure S10.** Experimental XANES spectra of bulk PdO reference (red), commercial Pd(OH)<sub>2</sub>/C Pearlman's catalyst (green), and Pd foil (grey) collected during the independent experiment at BM26A beamline of ESRF.

The BM31 beamline of ESRF allows for quasi-simultaneous measurements of XAS and XRD data. This possibility was exploited during the experiment to monitor possible changes due to formation of oxidic and metallic phases of palladium. However, the low crystallite size of palladium nanoparticles and low Pd loading did not allow us to distinguish any Pd-related reflections behind the Al<sub>2</sub>O<sub>3</sub> ones. The absence of Pd reflection again confirms the ultra-small size of nanoparticles.

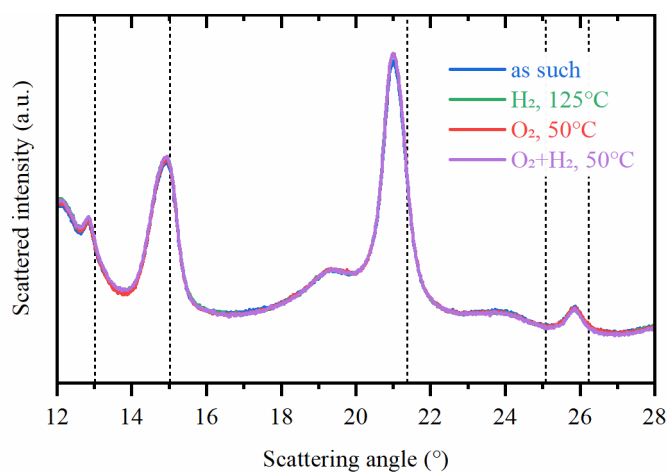


**Figure S11.** XRD profiles ( $\lambda = 0.5111 \text{ \AA}$ ) collected quasi-simultaneous with XAS spectra for oxidized sample at room temperature (region 1 in Figure 3b of the main text), after reduction in H<sub>2</sub> at 125 °C (region 3), subsequent re-oxidation (region 3) and during the reaction (region 5). Vertical dashed lines are located at angles where metallic palladium reflections are expected.

Mass spectroscopy data were collected continuously during XAS and XRD measurements. Selected signals with  $m/Z$  of 2, 4, 18 and 32 are shown in Figure S12. During the activation (region 2), formation of water was observed upon heating indicating the removal of oxygen from oxidized palladium particles. After re-oxidation of palladium surface (region 4), small signal of water was again detected in hydrogen flow. A stronger signal of water was then observed under catalytic conditions (region 5), but the activity decreased slightly with time. After removing of oxygen from the gas feed, the water signal starts to increase which may be related to the partial reduction of palladium surface. It should be noted that visible amounts of water were condensed inside the capillary after the sample, which explains why the water signal remains even after continuous flow of H<sub>2</sub>/He mixture.

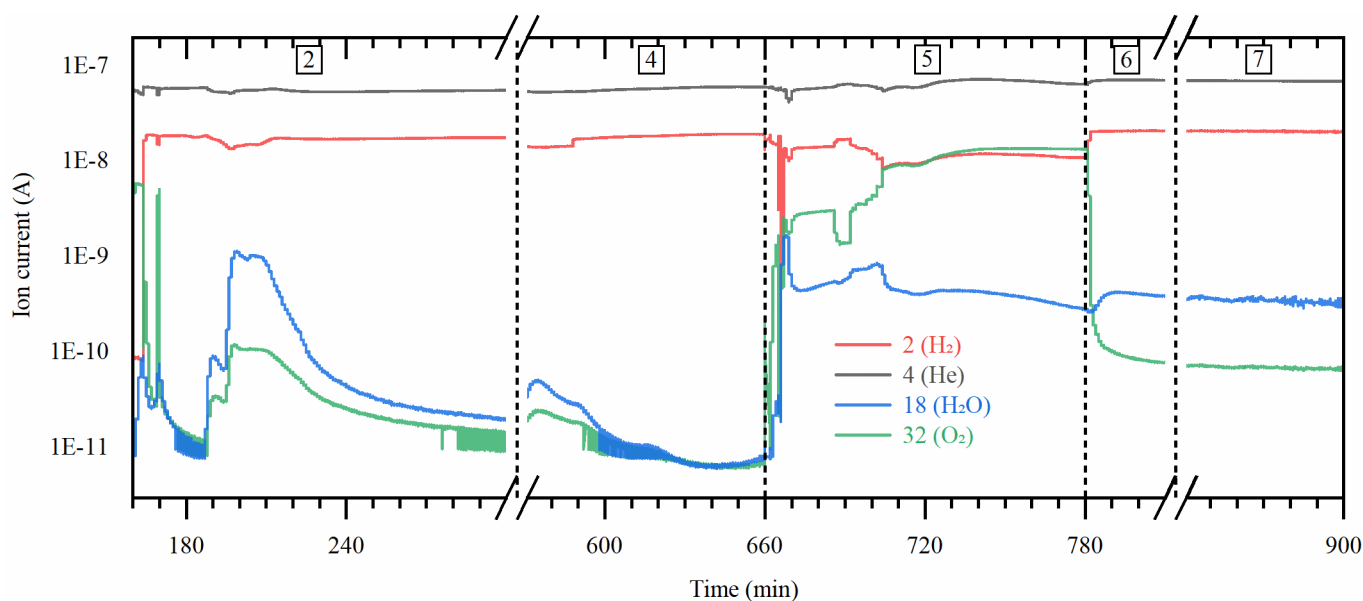


**Figure S12.** Mass spectroscopy data for  $m/Z$  of 2, 4, 18 and 32 collected during *in situ* synchrotron experiment.



## Temperature increase during H<sub>2</sub> oxidation

To estimate the temperature increase due to hydrogen oxidation reaction, two experimental tests summarized in Figure S13 have been performed. These tests were done independently from XAS measurements under similar conditions with a thermocouple inserted directly in the catalyst powder. In the first experiment (Figure S13a), the catalyst was continuously exposed to 10 vol. % H<sub>2</sub> in argon at 50 °C, and the pulsed injections of (0.5 ml each) of 10 vol. % O<sub>2</sub> in helium were performed. As can be seen from the figure the heat realized takes place during each injection resulting in the temperature increase by ca. 1 °C. In the second test, after continuous exposure to 10 vol. % H<sub>2</sub> in argon, the gas composition was changed to 5% H<sub>2</sub> and 5% O<sub>2</sub> (the area highlighted by blue background in Figure S13b). The temperature increased rapidly, and the sample was kept in the catalytic mixture for ca. 5 min until the temperature was stabilized at 77 °C. After the gas was switched back to 10% H<sub>2</sub>, a short increase of temperature to 83 °C was observed which might be related to reduction of surface oxide and correlates with the MS observations performed during XAS experiment. It is important to note, that the maximal temperature during reaction remained low enough to allow potential adsorption of hydrogen by Pd NPs.

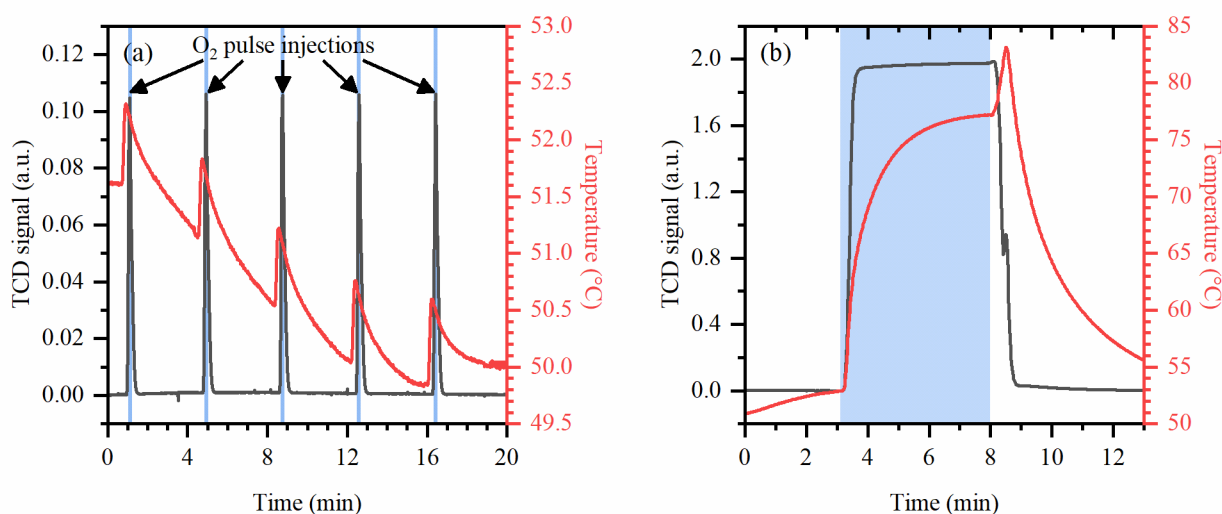


**Figure S13.** Temperature (red curves, right ordinate axes) and TCD signal (black curves, left ordinate axes) during pulsed injections of O<sub>2</sub> (a) and continuous exposure to the O<sub>2</sub> + H<sub>2</sub> mixture (b). The white background corresponds to 10% H<sub>2</sub> gas feed. The blue background corresponds to injection of 0.5 ml of 10 vol. % O<sub>2</sub> in part a, and a gas feed of 5% H<sub>2</sub> and 5% O<sub>2</sub> in part b.

## References

1. W. van Beek, O. V. Safonova, G. Wiker and H. Emerich, *Phase Transit.*, 2011, **84**, 726-732.
2. B. Ravel and M. Newville, *J. Synchrotron Radiat.*, 2005, **12**, 537-541.
3. S. Calvin, M. M. Miller, R. Goswami, S. F. Cheng, S. P. Mulvaney, L. J. Whitman and V. G. Harris, *J. Appl. Phys.*, 2003, **94**, 778-783.
4. M. W. Tew, J. T. Miller and J. A. van Bokhoven, *J. Phys. Chem. C*, 2009, **113**, 15140-15147.
5. V. V. Srabionyan, A. L. Bugaev, V. V. Pryadchenko, L. A. Avakyan, J. A. van Bokhoven and L. A. Bugaev, *J. Phys. Chem. Solids*, 2014, **75**, 470-476.
6. G. Kresse and J. Furthmuller, *Phys. Rev. B*, 1996, **54**, 11169-11186.
7. G. Kresse and D. Joubert, *Phys. Rev. B*, 1999, **59**, 1758-1775.